Rare Metal Materials and Engineering
Volume 52, Issue 4, April 2023
Available online at www.rmme.ac.cn

Science Press

Cite this article as: Liu Quanbing, Liu Zongde, Wang Yongtian, et al. Effect of Cr Addition on Corrosion Resistance of Laser-Cladding Ni-Cr-Mo Coatings in Chloride Solution with Thiosulfate[J]. Rare Metal Materials and Engineering, 2023, 52(04): 1210-1218.

ARTICLE

Effect of Cr Addition on Corrosion Resistance of Laser-Cladding Ni-Cr-Mo Coatings in Chloride Solution with Thiosulfate

Liu Quanbing, Liu Zongde, Wang Yongtian, Kong Yao, Ma Herong, Li Yue

Key Laboratory of Power Station Energy Transfer Conversion and System of Ministry of Education, North China Electric Power University, Beijing 102206, China

Abstract: The effect of Cr addition on the corrosion resistance of the laser-cladding Ni-Cr-Mo coatings was evaluated in chloride solution with thiosulfate by microstructure observation and electrochemical measurements. Results show that very similar microstructures and phase compositions are tested by scanning electron microscope and X-ray diffraction. Both eutectic and dendrite structures are observed, and the coatings are mainly composed of the γ-Ni solid solution of Cr, Mo, W, Fe, and Cr0.19Fe0.7Ni0.11 solid solution. The electrochemical results confirm that the laser-cladding coating with the special Cr addition behaves better corrosion resistance. The coating C28 performs higher values in open circuit potential and lower passive current density, especially the larger modulus of the impedance and charger transfer resistance. With increasing Cr content, the passive film is much thicker and the defects of the films are less in chloride solution with thiosulfate. The Mott-Schottky reveals that the passive film formed on the top surface of the laser-cladding coatings in solution behaves as n-type and p-type semiconductors.

Key words: laser cladding; microstructures; electrochemical behavior

Hastelloy C22 is a kind of high nickel base alloy that has been used in a wide range of industrial applications for its superior corrosion resistance to localized corrosion[1]. Abundant studies have been undertaken to investigate the properties of passive film on Hastelloy C22 in highly corrosive environments[2–4]. However, Hastelloy C22 needs to be imported and its high cost limits its large-scale applications. Laser cladding has provided another effective and promising method to develop the Hastelloy C22 coating with excellent mechanical and anticorrosive properties[5] in recent decades. The coating[6] produced by laser cladding is metallurgically well-bonded with the substrate and has the advantages of low dilution, small heat-affected-zone, and low distortion of the substrate. From the interface between laser-cladding Hastelloy C22 coating and steel substrate to the top surface of the coatings, the microstructure has been investigated by Wang et al[7]. Additionally, increased laser scanning speed improves the corrosion resistance of laser-cladding C22 coating due to the existence of smaller grain and lower dilution rates of Ni and Fe[8]. Besides, various corrosive environments have been designed to evaluate the corrosion resistance of C22 coating[9] produced by laser cladding. Wang et al[10] evaluated the erosion-corrosion behavior of C22 coating in static and cavitation acid solutions. Chen et al[11] used a self-designed impingement device to investigate the relationship between corrosion rate and impingement angle, velocity, and vibration frequency.

Based on previous studies[12–14], it was found that alloying elements play an essential role in the stability of the passive film and its repassivation kinetics. Chromium (Cr) was added to form a barrier oxide layer on the surface to prevent metals from reacting under the corrosive environment[15]. However, the passive oxide films will eventually destabilize when corrosion media contained chloride and thiosulfate ions[16–17]. In this sense, chloride ions broke down the passive film at first, then a small number of thiosulfate ions reacted with the passive film to accelerate the pitting corrosion[18]. It was reported that the synergistic effect of chloride ions and

Received date: August 10, 2022
Corresponding author: Liu Zongde, Ph. D., Professor, School of Energy, Power and Mechanical Engineering, North China Electric Power University, Beijing 102206, P. R. China, Tel: 0086-10-61772812, E-mail: lzd@ncepu.edu.cn

thiosulfate on pitting corrosion depends on the concentration ratio of these two ions[19]. Efforts have been made to improve the corrosion resistance of laser-cladding coatings in sulfuric acid environments by optimizing the Cr contents[20]. However, little attention is focused on the effect of Cr addition on the corrosion behavior of Ni-Cr-Mo coatings[21–22] fabricated by laser cladding technique in the aggressive solution containing chloride and thiosulfate ions.

This study explored the effect of Cr addition on the corrosion resistance of laser-cladding Ni-Cr-Mo coatings. The microstructural observation was carried out to link the change in the microstructure with the corrosion behavior of coatings with varying Cr content. The electrochemical measurements were conducted to evaluate the corrosion property of coatings in chloride solutions with thiosulfate.

1 Experiment

Q235 steel was used as a substrate material, and laser cladding powder was: C22 alloy powder, 97wt% C22 alloy powder +3wt% pure Cr powder, 95wt% C22 alloy powder+ 5wt% pure Cr powder, 92wt% C22 alloy powder+8wt% pure Cr powder, corresponding to the powder and coatings named as C22, C24, C26, and C28, respectively. The powder proportionally mixed was placed into stainless steel ball milling containers at 200 r/min for 12 h to mix and pulverize. The chemical composition of the substrate and powder is listed in Table 1. The multilayer laser cladding coatings were fabricated by a fiber laser system (zKzM-RF-3000, China) with a power of 2.5 kW, and the laser cladding parameters are given in Table 2. After laser cladding, the as-prepared coatings were cut into 10 mm×10 mm×5 mm. Specimens for corrosion tests were mounted in epoxy resin with an exposure area of 1.0 cm^2. The cross-section and work surface of the specimen were polished with diamond paste after being ground up to 2000 grits sequentially with SiC abrasive papers. Finally, the samples were ultrasonically cleaned in acetone for 10 min and then dried for the test. The thickness of coatings after surface treatment was about 1500 μm.

The microstructure of the laser-cladding coatings was analyzed by FEI Quanta 200F scanning electron microscope (SEM) operated at an accelerating voltage; the element composition and distribution were detected by energy dispersive X-ray spectroscopy (EDS). Before observation, the sample surface was eroded to reveal the microstructure of cladding composite coating with aqua regia solution (3HCl: HNO_3, v: v). In addition, the phase composition of the laser cladding coatings was analyzed by an X-ray diffraction device, which was operated at a scanning speed of 8°/min at 20 kV and 10 mA, and the diffraction angle 2θ was from 20° to 100°.

The electrochemical measurements were performed by the electrochemical workstation (CHI 660E, Chenhua, Shanghai) with a conventional three-electrode electrochemical glass cell, consisting of a working electrode of the laser-cladding coating, a reference electrode of saturated calomel electrode (SCE), and a counter electrode of platinum. Additionally, a lugging capillary was used to minimize *IR* drop, and all potentials were referred to the SCE. The test solutions (pH= 6.84) used were 0.6 mol/L chloride plus 0.1 mol/L sodium thiosulfate. Before the test, the working electrodes were polarized potentiostatically at –1 V_{SCE} for 10 min to remove air-formed oxides. The samples were immersed in chloride solution with thiosulfate for 1 h to attain a stable open circuit potential (OCP) before testing polarization curves, electrochemical impedance spectroscopy (EIS), and Mott-Schottky experiments.

Potentiodynamic polarization curves were measured from –300 mV (vs. OCP) to 1000 mV with a scan rate of 0.5 mV/s. EIS measurements were conducted over a frequency ranging from 10^5 Hz to 10^{-2} Hz at stable open circuit potential with amplitude sinusoidal voltage of ±10 mV. The software ZsimpWin was used to analyze EIS data. Mott-Schottky experiments were conducted to investigate the properties of the passive films by measuring the potential from –0.4 V_{SCE} to 1.0 V_{SCE} with a sweep rate of 20 mV at a frequency of 1000 Hz with an amplitude signal of 10 mV. All the measurements were performed under ambient temperature (25±2 ° C) and opened to air. Each experiment was repeated three times to ensure reproducibility.

Table 1 Chemical composition of Q235 steel and different laser-cladding powders (wt%)

Material	Cr	Mo	W	Fe	Co	C	Ni	Si	Mn	S	P
Q235 steel	-	-	-	Bal.		0.16		0.30	0.35	0.04	0.04
C22	22.0	14.0	3.5	5.6	0.75	0.01	Bal.	-	-	-	-
C24	24.3	13.6	3.4	5.4	0.73	＜0.01	Bal.	-	-	-	-
C26	25.9	13.3	3.3	5.3	0.71	＜0.01	Bal.	-	-	-	-
C28	28.2	12.9	3.2	5.2	0.69	＜0.01	Bal.	-	-	-	-

Table 2 Laser cladding parameters

Parameter	Value
Spot diameter/mm	2
Laser scanning rate/cm·s^{-1}	10
Overlap ratio/%	70
Powder feeding rate/kg·h^{-1}	1.8
Argon gas flow/mL·min^{-1}	15

2 Results and Discussion

2.1 Microstructure and phase analysis of laser-cladding coatings

The microstructure of the top surface of the coatings after erosion treatment is shown in Fig. 1. The structure of each

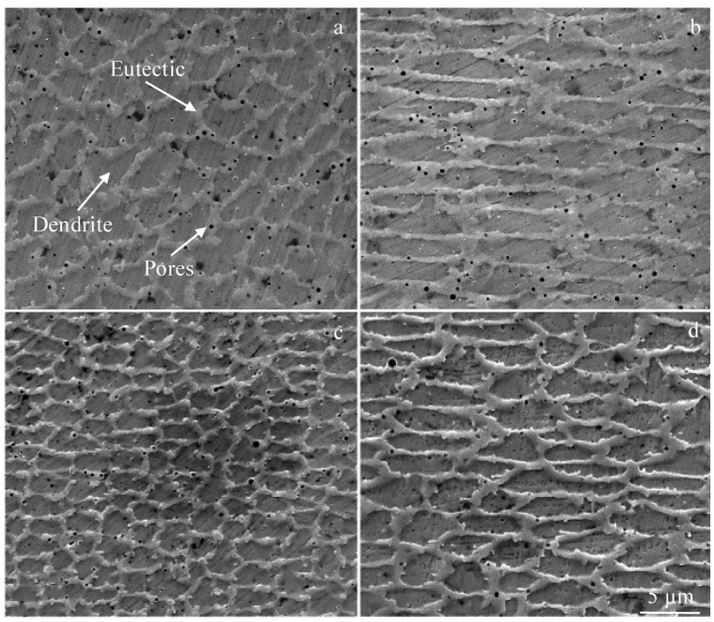

Fig.1 Microstructures of the top surface of the cladding coatings after erosion treatment: (a) C22, (b) C24, (c) C26, and (d) C28

coating is mainly composed of eutectic and dendrite. Very similar element distributions have been tested by EDS mapping for all coatings. The element distributions of coating C28 are representative (Fig. 2). It indicates that eutectic and dendrites are composed of Ni, Cr, Mo, W, and Fe on the surface of the coating, and Ni, Cr, and Mo are uniformly distributed in eutectic and dendrite, while W is mainly distributed in eutectic solidification. The contents of element Cr are similar in eutectic and dendrite and increase with the addition of Cr contents. The high content of Cr significantly thickens the passive film of Cr oxide and improves the corrosion resistance of the passive film. Moreover, few defects of porosity are observed in eutectic networks. It has been reported that micro-pores exist because gas can be trapped in the form of bubbles in the melt pool when the front wall solidifies[23].

Similar diffraction peaks in the XRD patterns of laser-cladding coatings (Fig. 3) can be detected for four samples, which indicates that γ-Ni solid solution and $Cr_{0.19}Fe_{0.7}Ni_{0.11}$ solid solution (PDF#33-0397) are the primary phases in the cladding coatings. But the diffraction peaks of γ-Ni solid solution move a little towards the left compared with the XRD standard diffraction card (PDF#04-0850). Because the atomic radius of Cr, Mo, W, and Fe is larger than that of Ni, the lattice will be distorted, and part of the crystal plane spacing will become larger when alloy elements substitute partial

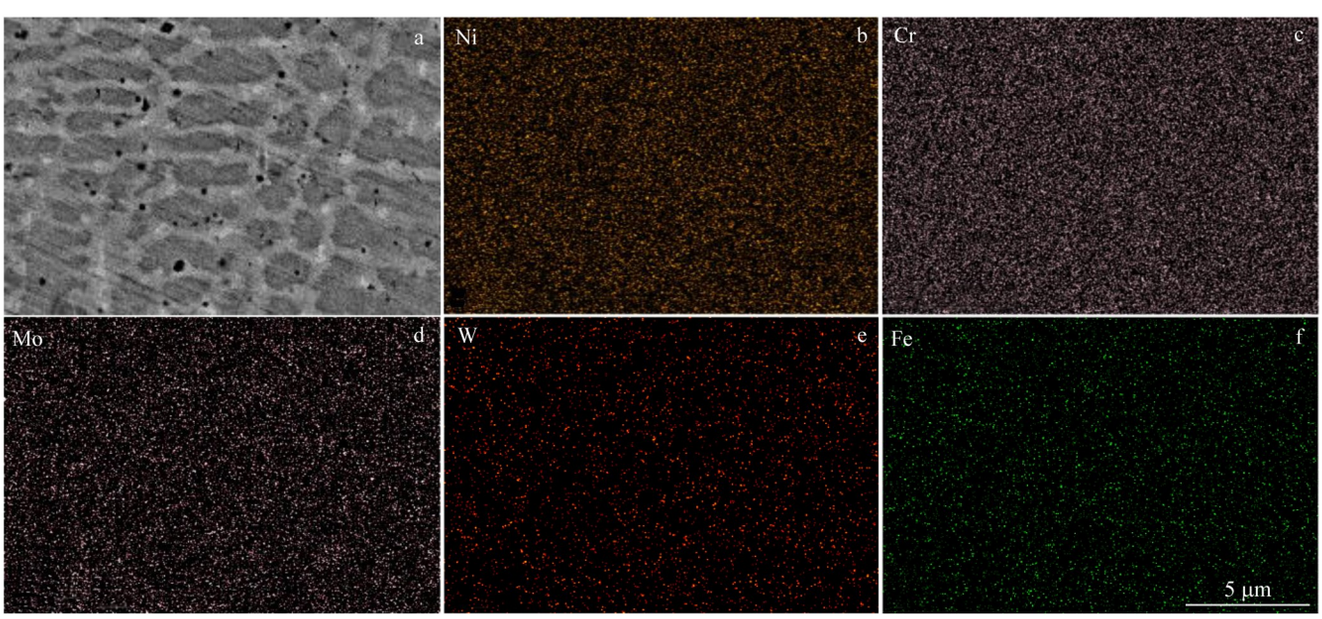

Fig.2 SEM image of cross-section (a) and EDS mappings (b–f) on top of coating C28

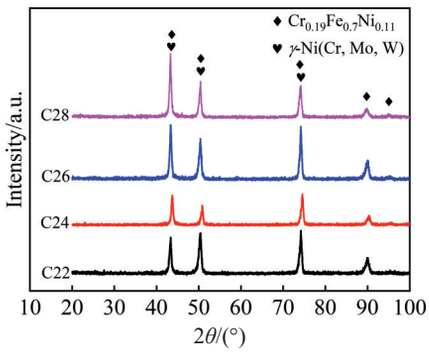

Fig.3 XRD patterns of cladding coatings

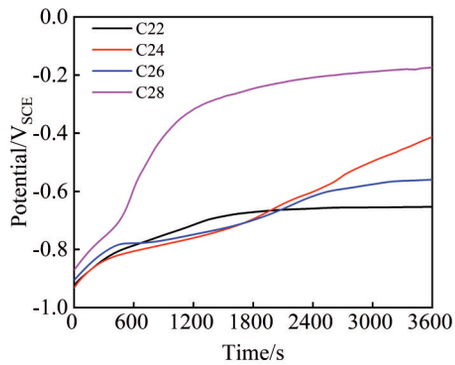

Fig.4 OCP curves of cladding coatings in chloride solution with thiosulfate

nickel atom in the face-centered cubic (fcc) γ-Ni phase to form the solid solution phase, leading to an increase in spacing (d) in Bragg equation ($2d\sin\theta=\lambda$). Therefore, the angle (θ) decreases, corresponding to the movement of diffraction peaks on the left. The diffraction peak intensity (2θ=43°) of the $Cr_{0.19}Fe_{0.7}Ni_{0.11}$ solid solution increases gradually with increasing Cr content, indicating that the ratio of the $Cr_{0.19}Fe_{0.7}Ni_{0.11}$ phase increases. The phase of the carbide is not detected because of the low content of the C element.

2.2 Corrosion behavior of cladding coatings

2.2.1 OCP and potentiodynamic polarization

The OCP values of the coatings listed in Table 3 are obtained from the average value of the open circuit potential curves for the last 300 s in Fig.4. It can be observed that the potentials increase with time in the beginning and then reach a steady state, where the change rate of the OCP values is less than 5 mV/min at the last 300 s. Generally, the positive shift of OCP curves is related to the growth process of the passive film under freely-corroding conditions. There is a trend that the potential increase rate of coating C22 is lower than that of other coatings in chloride solution with thiosulfate. In a steady state, the OCP value of the coating C22 is –653 mV_{SCE}, while that of coating C28 reaches – 177 mV_{SCE}, due to the higher content of Cr, which can benefit the passivation film formation[24] in the coating C28. Because the passive film is mainly composed of chromium oxides[25], consisting of a Cr(III)-dominated barrier layer and an outer dominantly-hydroxide layer, it can be found from the Pourbaix diagram of chromium in the Cr-H_2O system at 25 °C that chromium exhibits corrosion resistance due to the existence of protective oxide of the Cr_2O_3.

The potentiodynamic polarization curves of the laser-cladding coatings in chloride solution with thiosulfate are presented in Fig. 5. The electrochemical parameters obtained from the curves are listed in Table 3, including corrosion potential (E_{corr}), passive potential (E_p), passive current density (i_p) and breakdown potential (E_b). E_b is a potential at which the current density reaches a value of 10^{-4} A·cm^{-2}[26] and it represents the transition from passive to transpassive behavior. Passive current density (i_p) characterizes the dissolution rate of the passive film in the passive potential region.

Table 3 Electrochemical parameters of cladding coating samples in chloride solution with thiosulfate

Sample	OCP/ mV_{SCE}	E_{corr}/ mV_{SCE}	i_p/ μA·cm^{-2}	E_p/ mV_{SCE}	E_b/ mV_{SCE}
C22	−653	−624	49.23	−214	872
C24	−416	−114	4.68	158	809
C26	−560	−305	2.62/9.52	−104	850
C28	−177	−117	1.18	141	814

Therefore, a lower passive current density means a lower dissolution rate of the passive film in a chloride solution with thiosulfate. The passive current densities of the coatings C24, C26, and C28 decrease compared with the coating C22, indicating that the corrosion resistance of the coatings increases in the test environment with the addition of Cr. In particular, the coating C28 exhibits the lowest passive current density, suggesting the highest corrosion resistance when the Cr content is about 8wt% in this study.

As observed in Fig.5, the passive region obtained in coating C22 is wider due to the negative corrosion potential, which presents the corrosion tendency in thermodynamically controlled conditions. The coating C22 begins to passivate at –214 mV_{SCE} while the coatings C24, C26, and C28 start to be passive at more positive potential. It is believed that the decreased corrosion potential is attributed to the inhibition of the cathodic process or the acceleration of the anodic process.

It can be seen from Table 3 that the E_{corr} values are higher than OCP values in chloride solution with thiosulfate except for coating C22. Generally, the passive film is formed on the coating surface during the OCP measurement. In polarization curve measurement, the pre-existing passive film formed on the coating surface can be removed partially by the cathodic scan, which leads to a decrease in the potential of the oxide layer. However, the result is different from this phenomenon. Because of the increased Cr content, the formation rate of passive film is greater than the dissolution rate during the cathodic scan process.

It is noteworthy that the passivation process of coating C26 consists of two regions, the passive region (I) and (II). The passive region (I) is located between – 104 mV_{SCE} and 157 mV_{SCE}, while the passive region (II) is between 157 mV_{SCE} and

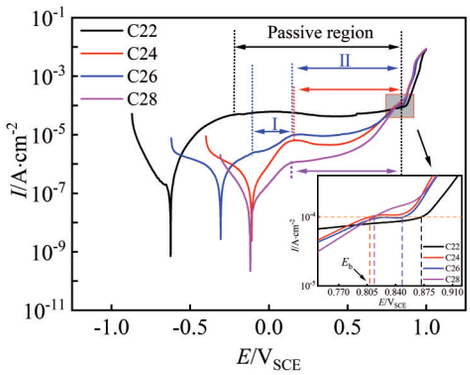

Fig.5 Potentiodynamic polarization curves of the cladding coatings in chloride solution with thiosulfate

850 mV$_{SCE}$. Therefore, the passive current density of coating C26 is 2.62 and 9.52 μA·cm^{-2} for the first and secondary passivation process (Table 3), respectively. This passivation behavior may be due to competitive adsorption. In the passive region (I), as the potential sweeps to more positive region, current density becomes observable near 157 mV$_{SCE}$. When the current density increases slowly as the potential increases, the development of pitting corrosion is slow, demonstrating that the passivation state of the coating surface has not been seriously damaged, which is still in the early stage of pitting development. Thiosulfate ions adsorbed can block the channel of aggressive chloride ions and inhibit the development of pitting corrosion. As a result, the current density stops rising and remains stable, forming a unique peak of "secondary passivation".

The surface morphology of the cladding coatings was investigated (Fig.6) after potentiodynamic polarization ending with 1 V in chloride solution with thiosulfate. The dendrite is dark while the eutectic is bright, and EDS results of points are listed in Table 4. The results indicate that the phases are S-related species and Cl^- are not detected, which is possibly related to adsorption on the surface of the passive film after the electrochemical reduction of thiosulphate. Moreover, it is observed that white granular phases mainly occur at the eutectic solidification, and white phases contain elements such as Ni, Cr, Mo, Fe and W. The defects of porosity decrease, covered with more white phases with the increase in Cr content in the cladding coating.

2.2.2 Electrochemical impedance spectra

It is apparent in Fig. 7a that the Nyquist plots of the

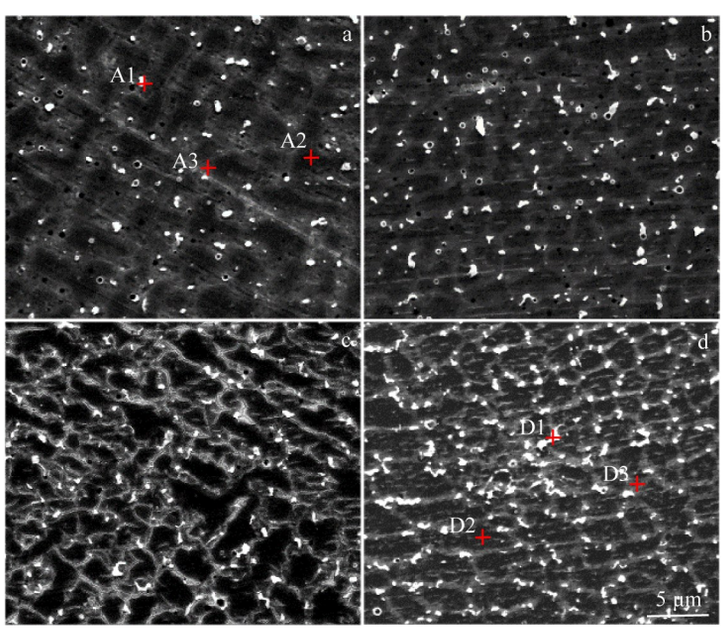

Fig.6 SEM morphologies of cladding coatings after potentiodynamic polarization in chloride solution with thiosulfate: (a) C22, (b) C24, (c) C26, and (d) C28

Table 4 EDS analysis results of different points marked in Fig.6 (wt%)

Coating	Point	C	O	W	Mo	S	Cr	Fe	Ni
C22	A1	5.35	6.26	6.02	11.25	0.89	19.35	4.87	46.00
	A2	5.50	5.07	6.44	12.85	0.93	19.79	4.71	44.71
	A3	5.21	6.63	6.86	16.21	1.24	19.54	4.34	39.95
C28	D1	5.60	5.40	6.64	15.15	1.03	22.98	3.96	39.24
	D2	4.84	6.67	6.42	10.91	0.71	21.72	4.18	44.54
	D3	5.05	6.13	5.86	13.82	0.67	23.30	4.19	40.98

cladding coatings display the same shape, indicating a similar passive mechanism. The semi-circles at the region of high frequencies are generally associated with the charge transfer at the electrode/electrolyte interface, which indicates the interface resistance of the charge transfer. Therefore, the diameters of the capacitive semi-circles present the corrosion resistance of the passive film in the corrosive media. According to the Nyquist plots, it can be concluded that the cladding coating C28 exhibits the best corrosion resistance of the passive films due to the largest semi-circle arc diameter.

It is clearly observed that the modulus of the impedance of the coatings with the addition of Cr is larger than that of the coating C22 from the Bode plot (Fig. 7b). The phenomenon that the phase angles reach their maximum values in the region of intermediate frequencies is a characteristic response of capacitive behavior[27]. In particular, coating C28 performs the largest modulus of the impedance due to the formation of a more stable passive film, and its phase angle tends towards −80° over a wide range of frequencies. The Bode-phase plots of the cladding coatings display two overlap time constants which are not easily distinguished in the high and intermediate frequency range. The time constant in the high-frequency region reflects the occurrence of the charge transfer reaction at the film-electrolyte interface, and the time constant in the intermediate frequency region is related to the properties of the porous film with finite thickness or relaxation in a space charge layer, whereas the low-frequency region is associated with the mass-transfer.

An equivalent electric circuit (Fig. 7c) has been established for fitting the impedance spectra data. The physical significance of the model has been described in Ref. [28–29]. In the equivalent electric circuit, the symbol Q has been widely utilized to signify the possibility of a non-ideal capacitance (CPE, constant phase element). When there are defects on the electrode surface, such as surface roughness, grain boundaries, distribution of the active sites, adsorption of inhibitors, and formation of porous layers[30], they result in surface heterogeneity. Therefore, the electrode surface deviates from the ideal capacitance. The impedance of parameter Q is defined as:

$$Z_{CPE} = Z_0(i\omega)^{-n} \quad (1)$$

where Z_0 represents the Q constant (CPE), Z_{CPE} represents the impedance of the Q constant ($\Omega^{-1}\cdot cm^{-2}\cdot s^n$), ω is the angular frequency (rad/s), $i^2=-1$ is the imaginary number, and n is the Q exponent. The factor of n is an adjustable parameter between 0 and 1. According to changes in the n value, Q can represent different physical significance. When n=0, Q represents the resistance; for $0.5<n<1$, Q reflects the distribution of dielectric relaxation time in frequency space; Q represents a Warburg impedance with diffusion character when n =0.5; and ideal capacitance is considered when n =1.

In Fig. 7c, R_s represents the solution resistance, R_f stands for the resistance due to the ionic paths through the oxide film, and Q_f represents the capacitance of the passive film formed. C_{dl} has been replaced by Q_{dl} to describe the capacitance of the electric double layer, which is usually attributed to surface heterogeneity, and R_{ct} corresponds to the charge transfer resistance of the double layer. This model is considered as an inhomogeneous layer rather than a defective layer based on the hypothesis that the passive film is not completely broken down. Therefore, this model is more suitable for the cladding coatings to explain the corrosion resistance mechanism in the interface of electrolyte/passive film/coating.

The fitting parameters are listed in Table 5. The fitting results show that a decrease in Q_f is accompanied by an increase in R_f, suggesting that the passive layer becomes thicker and more protective with the addition of Cr in coating C22. The Q_{dl} reflects the compactness of the passive film or corrosion layer. The value of the exponent n_2 of the coating C22 is 0.91, suggesting that the passive film surface is

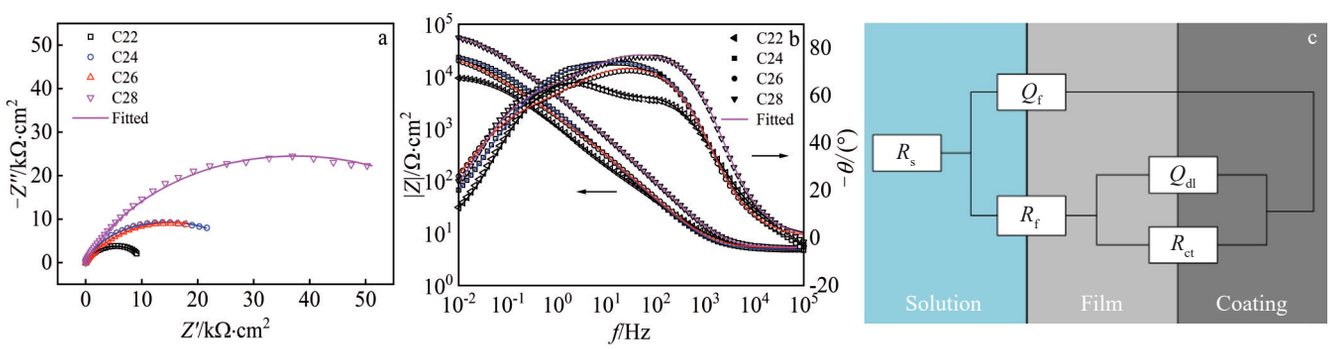

Fig.7 Nyquist plots (a) and Bode plots (b) of cladding coatings in chloride solution with thiosulfate and corresponding equivalent circuit (c)

Table 5 Equivalent circuit parameters for electrochemical impedance spectra

Coating	R_s/Ω·cm²	$Y_{o,1}$/×10⁻⁴ Ω⁻¹·cm⁻²·sⁿ	n_1	R_f/Ω·cm²	$Y_{o,2}$/×10⁻⁴ Ω⁻¹·cm⁻²·sⁿ	n_2	R_{ct}/kΩ·cm²
C22	4.847	1.81	0.76	510	0.32	0.91	10.22
C24	4.845	0.99	0.85	1163	1.12	0.54	19.53
C26	5.219	0.97	0.84	2785	1.11	0.60	29.04
C28	5.388	0.34	0.89	4929	0.36	0.64	71.81

homogeneous. Nevertheless, the values of the exponent n_2 are between 0.54 and 0.64 for the coatings C24, C26, and C28, which shows that the Q_{dl} has a character of Warburg impedance, also suggesting an inhomogeneity of the passive film surface. R_{ct} increases significantly with the addition of Cr in coating C22, indicating the gradual growth of the passive film, and also suggesting a slower rate of reactions taking place at the passive film/coating interface.

The thickness of the oxide film is a parameter influencing the barrier properties of the passive layer[31]. For the parallel plate capacitor model of a homogeneous oxide layer, the thickness of the passive film layer can be estimated with an impedance signal by the following equation[32]:

$$d = \frac{\varepsilon\varepsilon_0 A}{C} \tag{2}$$

where d is the thickness of the passive film layer (nm), ε_0 is the permittivity of vacuum (8.85×10^{-12} F·m^{-1}), ε is the dielectric constant (18), A is the effective area of the sample, and C is the capacitance of the passive film. Based on the fitting parameters (Q_f), the capacitance can be calculated by the following equation[33]:

$$C = \left(R_f^{1-n} Q_f\right)^{\frac{1}{n}} \tag{3}$$

where the R_f is the passive film resistance, Q_f is a constant phase element ($\Omega^{-1}\cdot cm^{-2}\cdot s^n$), and n is the exponent of the Q_f. According to Eq. (2) and Eq. (3), the estimated values of passive film thickness in the test solution are shown in Table 6. The values of passive film thickness formed on the coatings C24, C26, and C28 are larger than that formed on the coating C22, and the coating C28 reaches a maximum thickness of 5.08 nm in the test solution, suggesting that the coating C28 has the best corrosion resistance in chloride solution with thiosulfate among these coatings. This trend is in good agreement with the impedance results.

2.2.3 Mott-Schottky analysis

The Mott-Schottky was applied to characterize the semiconductive property and the density of charge carriers of the passive film formed on the surface of the coating. The space charge capacitance of n-type and p-type semiconductor is defined by Eq.(4) and Eq.(5), respectively:

$$\frac{1}{C^2} = \frac{2}{eN_D\varepsilon\varepsilon_0}\left(E - E_{FB} - \frac{kT}{e}\right) \tag{4}$$

$$\frac{1}{C^2} = -\frac{2}{eN_D\varepsilon\varepsilon_0}\left(E - E_{FB} - \frac{kT}{e}\right) \tag{5}$$

where e is the absolute value of the electron charge (1.602×10^{-19} C), ε is the relative dielectric constant of the semiconductor (20, which was estimated by Raja et al[34]), ε_0 is the vacuum permittivity of free space (8.854×10^{-14} F/cm), k is the Boltzmann constant (1.389×10^{-23} J/K), T is the absolute temperature, E_{FB} is the flat band potential which can be obtained from the extrapolation of $1/C^2$ to 0 V_{SCE}, N_D is the donor density (electron donor concentration for n-type semiconductor) and N_A is the acceptor density (hole acceptor concentration for p-type semiconductor).

The Mott-Schottky plots conducted under open circuit potential are shown in Fig. 8. There are some differences between coating C22 and other coatings with the addition of Cr. For coating C22, potentials from −0.4 to 0.45 V_{SCE} have the positive slopes representing n-type semiconductors, and potentials from 0.45 to 0.8 V_{SCE} have the negative slopes representing p-type semiconductors; while for other coatings, potentials from −0.4 to 0.3 V_{SCE} and 0.3 to 0.8 V_{SCE} present characteristics of n-type semiconductor and p-type semiconductor, respectively.

The donor and acceptor densities in semi-conducting passive layers are corresponding to the non-stoichiometry defects in the passive film, including cation vacancies, anion vacancies, and cation interstitials. The donor species are mainly oxygen vacancies or cation interstitials, while the acceptor species are cation vacancies. The transition from n-type to p-type is correlated to a change in the dominant point defect in the passive film. Different passive oxide layers formed on cladding coatings exhibit variable semiconductive properties, depending on the predominant defect present in the passive film. A layered structure[35] on the passive film of C22 alloy is tested, consisting of an inner layer rich in Cr and an outer layer enhanced in Mo. The Cr-rich inner layer, Cr_2O_3, in which Cr presents as Cr^{3+}, exhibits a p-type semi-conducting behavior.

The values of N_D and N_A determined from the slope of the experimental C^{-2} versus E plots are summarized in Table 7. Compared to the other coatings, the N_D value of coating C22

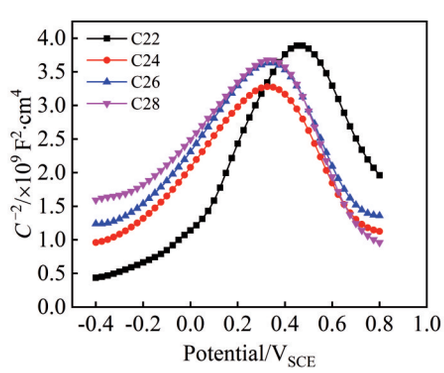

Fig.8 Mott-Schottky plots of passive films formed on cladding coatings in chloride solution with thiosulfate under open circuit potential

Table 6 Estimated passive film thickness of cladding coatings in chloride solution with thiosulfate

Coating	C22	C24	C26	C28
Thickness/nm	1.62	2.05	1.83	5.08

Table 7 Evolution of donor density (N_D) and acceptor density (N_A) calculated from Mott-Schottky experiments

Coating	$N_D/\times10^{20}$ cm^{-3}	$N_A/\times10^{20}$ cm^{-3}
C22	9.10	9.47
C24	15.46	9.43
C26	14.51	8.82
C28	17.16	7.53

is the lowest, indicating the lower dissolving rate of the cations at the interface of the passive film/solution. The decrease in N_A of coatings with the addition of Cr is attributed to decrease in diffusion rates of metallic ions and dehydration of hydroxide phases[36]. The addition of Cr increases the concentration of cation or anion vacancies inside oxides, preventing migration of cations from the metal substrate and penetration of harmful anions (Cl^-, $S_2O_3^{2-}$), to improve the corrosion resistance of the laser-cladding coatings.

3 Conclusions

1) The effect of Cr addition (3wt%, 5wt%, 8wt%) on the corrosion resistance of the laser-cladding Ni-Cr-Mo coatings is evaluated in the chloride solution with thiosulfate. From the substrate to the top surface of the specimen, the microstructure develops from planar solidification to cellular solidification and dendritic solidification. The structure of each coating in the middle and the top is mainly composed of eutectic and dendrite, where Ni, Cr, and Mo are well distributed while W is mainly distributed in eutectic solidification. γ -Ni solid solution and $Cr_{0.19}Fe_{0.7}Ni_{0.11}$ solid solution are the main phases in the laser-cladding coatings, and the ratio of $Cr_{0.19}Fe_{0.7}Ni_{0.11}$ phase increases with increasing Cr content.

2) Coating C28, added with 8wt% Cr, presents better corrosion resistance due to the growth of much thicker and less defective films. The potentiodynamic polarization curves suggest that coating C28 exhibits the highest corrosion resistance when Cr content is about 8wt% due to the lowest passive current density. Additionally, EIS results show that cladding coating C28 performs better corrosion resistance of the passive films due to the largest semi-circle arc diameter and modulus of the impedance with the growth of a much thicker passive film. Mott-Schottky analysis reveals that the passive film formed on the laser-cladding coatings in solution behaves as n-type and p-type semiconductors.

References

1 Ebrahimi N, Jakupi P, Korinek A *et al. Journal of the Electrochemical Society*[J], 2016, 163: 232

2 Ebrahimi N, Biesinger M C, Shoesmith D W *et al. Surface and Interface Analysis*[J], 2017, 49: 1359

3 Zagidulin D, Zhang X R, Zhou J G *et al. Surface and Interface Analysis*[J], 2013, 45: 1014

4 Abu Kassim S, Thor J A, Abu Seman A *et al. Corrosion Science*[J], 2020, 173: 108 761

5 Wang Q Y, Pei R, Liu S *et al. Surface and Coatings Technology*[J], 2020, 402: 126 310

6 Kong Yao, Liu Zongde, Li Bin. *Rare Metal Materials and Engineering*[J], 2021, 50(8): 2694

7 Wang Q Y, Xi Y C *et al. Transactions of Nonferrous Metals Society of China*[J], 2017, 27: 733

8 Wang Q Y, Zhang Y F, Bai S L *et al. Journal of Alloys and Compounds*[J], 2013, 553: 253

9 Kong Y, Liu Z D, Wang X Y *et al. Materials Today Communications*[J], 2022, 33: 104 603

10 Wang Q Y, Bai S L, Liu Z D. *Transactions of Nonferrous Metals Society of China*[J], 2014, 24: 1610

11 Chen L, Bai S L. *Applied Surface Science*[J], 2018, 437: 1

12 Zhang X, Zagidulin D, Shoesmith D W. *Electrochimica Acta*[J], 2013, 89: 814

13 Zadorozne N, Rebak R, Giordano M *et al. Procedia Materials Science*[J], 2012, 1: 207

14 Liu Hao, Gao Qiang, Hao Jingbin *et al. Rare Metal Materials and Engineering*[J], 2022, 51(6): 2199

15 Jakupi P, Wang F, Noël J J *et al. Corrosion Science*[J], 2011, 53: 1670

16 Xia D H, Song Y, Song S *et al. Journal of Tianjin University Science and Technology*[J], 2018, 51: 591 (in Chinese)

17 Zanotto F, Grassi V, Balbo A *et al. Corrosion Science*[J], 2018, 130: 22

18 Wu S, Wang J, Song S *et al. Journal of the Electrochemical Society*[J], 2017, 164: 94

19 Sun Y, Wu S, Xia D H *et al. Corrosion Science*[J], 2018, 140: 260

20 Zheng C, Liu Z D, Liu Q B *et al. Coatings*[J], 2022, 12: 421

21 Kong Y, Liu Z D, Liu Q B. *Journal of Thermal Spray Technology*[J], 2022, 31: 2136

22 Kong Y, Liu Z D, Wang X Y *et al. Journal of Alloys and Compounds*[J], 2023, 932: 167 536

23 Meng W, Li Z, Lu F *et al. Journal of Materials Processing Technology*[J], 2014, 214: 1658

24 Xu D D, Zhou B L, Wang Q Q *et al. Corrosion Science*[J], 2018, 138: 20

25 Mishra A K, Ramamurthy S, Biesinger M *et al. Electrochimica Acta*[J], 2013, 100: 118

26 Escriva Cerdan C, Blasco Tamarit E, Garcia Garcia D M *et al. Corrosion Science*[J], 2012, 56: 114

27 Della Rovere C A, Alano J H, Silva R *et al. Corrosion Science*[J], 2012, 57: 154

28 Chen L, Bai S L, Ge Y Y *et al. Applied Surface Science*[J], 2018, 456: 985

29 Boissy C, Ter Ovanessian B, Mary N *et al. Electrochimica Acta*[J], 2015, 174: 430

30 Luo H, Dong C F, Li X G *et al. Electrochimica Acta*[J], 2012, 64: 211

31 Feng Z, Cheng X, Dong C *et al. Corrosion Science*[J], 2010, 52: 3646

32 Orazem M, Tribollet B, Vivier V *et al. ECS Transactions*[J], 2013, 45: 15

33 Brug G J, Van Den Eeden A L G, Sluyters-Rehbach M *et al. Journal of Electroanalytical Chemistry and Interfacial Electrochemistry*[J], 1984, 176: 275

34 Raja K S, Namjoshi S A, Misra M. *Materials Letters*[J], 2005,

59(5): 570

35 Zhang X R, Qin Z, Zagidulin D *et al. Journal of the Electrochemical Society*[J], 2017, 164: 911

36 Huang J, Wu X, Han E H. *Corrosion Science*[J], 2010, 52: 3444

Cr添加对Ni-Cr-Mo激光熔覆层在含氯硫代硫酸盐溶液中耐蚀性的影响

刘泉兵，刘宗德，王永田，孔　耀，马何蓉，李　悦

(华北电力大学 电站能量传递转化与系统教育部重点实验室，北京 102206)

摘　要：通过微观结构观察和电化学测量，在硫代硫酸盐氯化物溶液中评估了Cr的添加对Ni-Cr-Mo激光熔覆涂层耐腐蚀性的影响。通过扫描电子显微镜和X射线衍射观察到了非常相似的微观结构和相组成。涂层主要有共晶和枝晶，并由包含Cr、Mo、W、Fe的γ-Ni固溶体和$Cr_{0.19}Fe_{0.7}Ni_{0.11}$固溶体组成。电化学结果表明，添加一定Cr含量的激光熔覆层表现出更好的耐腐蚀性。C28涂层表现出较高的开路电位值和较低的钝化电流密度，并且具有更大的阻抗模量和电荷转移电阻。随着Cr含量的增加，在含氯的硫代硫酸盐溶液中钝化膜的厚度变厚，膜的缺陷变少。Mott-Schottky分析表明，溶液中激光熔覆层上表面形成的钝化膜表现为n型和p型半导体。

关键词：激光熔覆；组织结构；电化学行为

作者简介：刘泉兵，男，1994年生，博士生，华北电力大学能源动力与机械工程学院，北京 102206，E-mail：quanbing21@126.com